Granular Matter (2010) 12:387–397
DOI 10.1007/s10035-010-0187-6

Hydrodynamic modeling of dilute and dense granular flow

Arnulf Latz · Sebastian Schmidt

Received: 4 May 2009 / Published online: 18 April 2010

Abstract We study numerically a continuum model for granular flow, which covers the regime of fast dilute flow as well as slow dense flow up to vanishing velocity. The constitutive relations at small and intermediate densities are equivalent to those derived from kinetic theory of granular flow. The existence of an inherent instability due to the vanishing kinetic or collisional pressure for small granular temperatures requires a cross over from a collisional pressure to an a thermal yield pressure at densities close to random close packing. Contrary to a kinetic viscosity, the viscosity turns into a function diverging for small temperatures analogous to the diverging viscosities of liquids close to the glass transition. In this respect the presented model is a simplified version of a model of Savage (J Fluid Mech 377:1–26, 1998), which nevertheless recovers many aspects of dense granular flow. As examples we show simulations of sandpiles with predictable slopes, hopper simulations with mass and core flow and angle dependent critical sand heights in flows down an inclined plane. We solve the system of the strongly nonlinear singular hydrodynamic equations with the help of a newly developed nonlinear time stepping algorithm together with a finite volume space discretization. The numerical algorithm is implemented using a finite volume solver framework developed by the authors which allows discretization on cell-centred bricks in arbitrary domains.

Keywords Complex fluids · Granular media · Non-Newtonian flows · Rheology

A. Latz · S. Schmidt (✉)
Fraunhofer ITWM, Kaiserslautern, Germany
e-mail: schmidts@itwm.fhg.de

1 Introduction

There is still no theory for the description of granular flow on a macroscopic scale with the same accuracy as the Navier Stokes equations for simple liquids. The main reasons are the existence of a very efficient mechanism for energy dissipation in the form of inelastic collisions and the lack of a clear time and spatial scale separation in the flow of granular material [2]. For weakly inelastic granular media kinetic theory provides a framework for deriving the correct hydrodynamic equations [3] under the usual assumption of molecular chaos and instantaneous collisions between grains. Although both assumptions might be violated for large energy dissipation [4,5] and despite of sometimes large spatially localized density fluctuations, the heuristically modified constitutive relations obtained from kinetic theory turn out to be a very useful tool for many simulations of granular flow in application problems at small and intermediate volume fractions as e.g. the simulation of fluidized beds [6] or hydrodynamic instabilities and pattern formation in granular gases [7,8]. For volume fractions close to the maximum packing fraction, the validity of kinetic theory becomes questionable, since the assumption of only collisional binary contacts between the grains is not valid anymore. Nevertheless striking good agreement between simulations [9,10] or experiments [11,12] at large volume fractions and hydrodynamic theory have been reported in the literature. The latter have especially shown that kinetic theory is able to mimic solid like behavior by exhibiting a solid like Coulomb stress as a solution of the hydrodynamic equations under shearing conditions. The existence of a dynamic Coulomb stress might explain why simulations and experiments under the condition of permanent driving as in the experiments or permanent input of energy via boundary conditions as in the molecular dynamic simulation can be reproduced by hydro-

dynamic theory at all. The proper theory of the stress for flowing granular media close to maximum packing fraction, where collisional contacts of grains are replaced by frictional contacts, would be some theory of static friction as e.g. the Coulomb friction theory. But, so it seems, the dynamic Coulomb friction of the hydrodynamic theory is able to mimic the true Coulomb friction, if there is permanent energy input to prevent the granular system from arresting.

In our paper we are also interested in situations where there is no permanent source of external energy to balance the internal dissipation. We will show that kinetic theory alone due to an inherent thermodynamic instability in certain flow conditions is not able to reproduce the resulting qualitative behavior of arresting flows like e.g. the formation of heaps during a filling process. Motivated by the work of Savage [1], we present a simplified hybrid model of kinetic theory and a theory derived from soil mechanics, which overcomes the difficulties observed in kinetic theories and extends the applicability of hydrodynamic theory to arresting granular flow. The obtained nonlinear hydrodynamic equations are solved with a newly developed nonlinear finite volume algorithm [13, Section 2.4]. We test the theory by simulating heap formation with predictable angle of repose, by comparing simulations of flow down an inclined plane with experiments and by reproducing core and mass flow in silos.

The paper is organized in the following way. In Sect. 2 we introduce the model in detail. In Sect. 3 an outline of the numerical algorithm is given. The potential of the model to reproduce essential properties of granular materials is demonstrated in Sect. 4. We conclude the results in Sect. 5.

2 Constitutive modeling

2.1 Conservation equations

We begin with the conservation equations for mass density ρ and momentum density $\mathbf{m} = \rho\mathbf{u}$ on a spatial scale which is large compared to the size of the grains, where $\mathbf{u}$ is the center of mass velocity.

$$\frac{\partial \rho}{\partial t} + \nabla(\mathbf{u}\rho) = 0 \tag{1}$$

$$\frac{\partial (\rho \mathbf{u})}{\partial t} + \nabla(\rho \mathbf{u} \otimes \mathbf{u}) = \nabla \underline{\underline{\sigma}} + \mathbf{f} \tag{2}$$

The tensor $\underline{\underline{\sigma}}$ is the total stress tensor including pressure and $\mathbf{f}$ is some external force density. It is convenient to split the stress tensor in scalar p and deviatoric part $\underline{\underline{\sigma}}^D$ by

$$\underline{\underline{\sigma}} = -p\underline{\underline{I}} + \underline{\underline{\sigma}}^D. \tag{3}$$

The velocity dependent part of the stress tensor is already contained in the convective term on the left hand side of the Eq. (2). There is no mechanism for sustaining deviatoric strain in the theory tested here, therefore the deviatoric stress will only depend on the strain rates, the state variables ρ and the granular temperature T. p will depend on density and granular temperature. In addition it is shown, that a contribution reminiscent of the trace of a strain rate tensor (see Sect. 2.4) is necessary to obtain stable physical solutions. To capture the granular aspects of the flow we make use of the granular temperature T as defined within the kinetic theory of granular flow [3]. In a constant pressure ensemble the equation for the granular temperature is given by (see Appendix. A)

$$c_p \rho \left(\frac{\partial T}{\partial t} + \mathbf{u} \nabla T \right) = -\hat{\rho}_s \nabla \mathbf{q} + \underline{\underline{\sigma}}^D : \underline{\underline{\kappa}} - \frac{3}{2} \rho \varepsilon T. \tag{4}$$

Here c_p, $\mathbf{q}$, ε are the granular specific heat at constant pressure per unit mass, the granular heat flux and the temperature dissipation rate due to inelastic interactions of the grains, respectively. $\underline{\underline{\kappa}}$ is the strain rate tensor, whose definition is given below in Eq. (8). The quantity $\hat{\rho}_s$ is the specific density of the grains. The expression for the specific heat at constant pressure c_p can be derived by transforming the standard equations at constant volume [3] to constant pressure. It is given by

$$c_p = \frac{3}{2} + \frac{p}{\rho^2} \left(\frac{\frac{\partial p_s}{\partial T}|_c}{\frac{\partial p_s}{\partial \rho}|_T} \right). \tag{5}$$

c_p converges to the ideal gas value $c_p = 5/2$ for $\rho \to 0$. Except for the last term, which describes the dissipation of granular temperature due to inelastic collisions, the Eq. (4) has the usual form of the heat transport equation [14]. The left hand side describes the change of granular temperature due to free streaming. On the right hand side the effects of diffusive temperature transport, viscous heating and dissipation are accounted for.

2.2 Constitutive equations from kinetic theory

To obtain a closed model, constitutive relations for the transport coefficients are necessary. The aim is to develop a model which is physically consistent and stable in the dilute regime as well as in the dense slow flow regime. In general it is not possible to rigorously derive constitutive models. Small and intermediate densities are well described by the constitutive relations from kinetic theory. Therefore it is possible to derive the hydrodynamic equations in this case and to obtain expressions for the stress tensor, the heat flux, all transport coefficients and the pressure [3,15]. Improved expressions for transport coefficients and equation of state may be obtained from molecular dynamic simulations [16–18]. An overview about the current state of modeling dense granular systems may be found in [19]. More complicated equations of state

apply for wet granular matter [20]. Since the hydrodynamic equations are derived using Chapman–Enskog theory the stresstensor and the heat flux are in lowest order linear in gradients of the hydrodynamic variables i.e.

$$\underline{\underline{\sigma}}^D = 2\eta \underline{\underline{\kappa}} \tag{6}$$

and

$$\mathbf{q} = -\lambda \nabla T, \tag{7}$$

with the non symmetrized strain rate tensor κ defined as

$$\kappa_{\alpha\beta} := \frac{\partial v_\alpha}{\partial x_\beta}. \tag{8}$$

The use of a symmetric stress tensor σ^D would have lead to so called mixed derivatives (i.e. derivatives of the form $\partial^2 u_x/\partial y \partial x$) in the resulting non linear Navier Stokes equation. Numerical tests showed that these derivatives cause large unphysical spreading of granular jets perpendicular to the flow direction, which motivated us to choose the non symmetrized form. A non symmetric stress tensor violates the conservation of angular momentum of the macroscopic flow field. Although it would be very hard to justify for simple liquids, this violation is not uncommon for hydrodynamic flow of fluids with internal rotational degrees of freedom [21,22] and is used for the modeling of collisional granular flow [23]. Friction between touching grains inhibits rotation of the grains and gives rise to a transfer of translational motion into rotations and vice versa. The latter mechanism can lead to a local dissipation of momentum. The unsymmetrized stress tensor is in this context motivated by defining a rotational viscosity η_R, which we chose to be equal to the shear viscosity i.e. $\eta_R = \eta$ and the definition of the stress tensor as

$$\sigma = \frac{\eta}{2}\left(\kappa + \kappa^T\right) + \frac{\eta_R}{2}\left(\kappa - \kappa^T\right). \tag{9}$$

Although the concept of rotational viscosity is used in the context of granular flow, we want to point out, that there are strong arguments against using non symmetric stress tensors [24]. We are especially not aware of any compelling argument to set the rotational viscosity equal to the shear viscosity, except for our numerical observation, that the simulations of granular jets look much more physical. But we also want to point out that for incompressible fluids with constant viscosity η the neglected part κ^T of the strain rate tensor does not contribute at all to the accelerating force due to

$$\frac{\partial}{\partial x_\beta}\left(\eta \kappa^T_{\alpha\beta}\right) = \frac{\partial}{\partial x_\beta}\left(\eta \frac{\partial v_\beta}{\partial x_\alpha}\right) = \eta \frac{\partial}{\partial x_\beta}(\mathrm{div}\, v) = 0. \tag{10}$$

We therefore expect, that in the dense regime of granular flow, where we have only a weakly compressible flow, our approximation does not influence the results too strongly.

The expressions for the transport equations also follow from kinetic theory. Their exact form is quite involved [15]. It was shown in [11,12], that quantitatively correct results can be obtained by a much simpler form of the equations. We therefore choose a similar form as in [11] for the expressions of the transport coefficients and the pressure, preserving the low density and high density limit. The kinetic expressions are denoted by the subscript K and are given as

$$p_K = T g(\rho)\rho \tag{11a}$$
$$\varepsilon_K := \varepsilon_0 \rho^2 \sqrt{T} g(\rho) \tag{11b}$$
$$\lambda_K := \lambda_0 \sqrt{T} g(\rho) \tag{11c}$$
$$\eta_K := \eta_0 \sqrt{T} g(\rho)^\beta, \tag{11d}$$

where

$$g(\rho) := \left(1 - \frac{\rho}{\rho_c}\right)^{-1} \tag{12}$$

is the value of the radial distribution function at contact. The kinetic or collisional pressure is an interpolation between the low density limit $p = \rho T$ and exhibits a divergence at $\rho = \rho_c$ found in simple kinetic theory (with Enskog corrections) [3]. The simulations show, that there is a need to have the same type of divergences in all three quantities in order to obtain stable unique solutions for the resulting equations (see Sect. 4.4). If a different approximation for the pressure with a different type of divergence is chosen (e.g. Carnahan Starling approximation [25]), all three quantities were to change in order to get stable solutions.

The bulk viscosity, which has a similar form as the shear viscosity except for a different small density behavior $\propto \rho^2$ was set to zero. Test simulations with a different version of our numerical code showed, that the use of a nonzero bulk viscosity did not qualitatively change our results. The exponent β was introduced in [11] to capture glassy aspects of the dense dynamics. In comparison with shearing experiments it was found to be between 1 and 2. We choose a value of $\beta = 1$, since our simulations showed that any value different than $\beta = 1$ had a very destabilizing effect on the formation of heaps in filling simulations (see Sect. 4.4). Recent results [17,18,26] seem to indicate that the viscosity diverges at a smaller density than other constitutive relations. Consequences of such a behavior on the numerical stability of complex hydrodynamic simulations remain to be tested.

2.3 Shortcomings of the kinetic constitutive equations

The kinetic constitutive equations seem to work quite well in a large range of densities. Phenomena like narrow albeit finite shearing zones, solid like stress behavior in steady shear flow and dependencies of height vs. angle for the gravity driven flow down an inclined plane can be calculated quantitatively [11,12]. Both physical situations have in common the continuing input of energy either via the application of a permanent torque or a permanent transformation of potential energy into

kinetic energy of the flow. In these situations there is always a nonzero granular temperature which guarantees that the purely thermal collisional pressure p_K Eq. (11a) stabilizes the system. Kinetic theory used for granular flow does not account for the strongly repulsive forces between the grains except for the Enskog corrections to pressure and transport coefficients in form of the radial distribution function at contact approximated by the function g in Eq. (11). But there is no athermal pressure independent of temperature.

If for any reason, the temperature reaches the zero limit faster than the density increases to the maximum packing fraction ρ_c, there is no force which prevents the system from collapse. This situation will for example occur when a box is filled and the grains are eventually coming to a rest. In this case the granular temperature vanishes and thus the collisional pressure, kinetic viscosity and stress. Due to the gravitational force in Eq. (2) no stationary solution for the velocity exists, if the temperature vanishes.

To understand how the state of zero temperature and maximum packing fraction is reached we investigate Haff's homogeneous cooling for the granular system described by Eqs. (4) and (11). Neglecting the gradients in the temperature and the velocities we obtain from (4)

$$c_p \frac{\partial T}{\partial t} = -\frac{3}{2}\varepsilon T. \tag{13}$$

For the final approach to the maximally packed state we can in leading order replace $c_p(\rho)$ by $c_p^c := c_p(\rho_c)$ and $\varepsilon(\rho, T)$ by ε^c with

$$\varepsilon^c := \varepsilon_0 \rho_c^2 \sqrt{T} g(\rho) \tag{14}$$

to obtain the equation

$$\frac{\partial T}{\partial t} = -\frac{3\varepsilon_0 \rho_c^2}{2c_p^c} g T^{3/2}. \tag{15}$$

Close to the maximum packing fraction the densities may be assumed to be constant [27] and Eq. (15) is solved by Haff's law

$$T(\rho, t) = \frac{T_0(1-(\rho/\rho_c))^2}{(1-(\rho/\rho_c) + A\sqrt{T_0}(t-t_0))^2} \tag{16}$$

with $A = \frac{3\varepsilon_0\rho_c^2}{4c_p^c}$. Using this expression for T in the collisional pressure p_K (Eq. 11a), we see that the pressure vanishes with the density approaching the maximum packing state $\rho = \rho_c$. In addition the system becomes thermodynamically unstable. This can be seen by calculating $dp_K(T(\rho, t))/d\rho$ using Eqs. (11a) and (16), which is for large times given by

$$\frac{dp_K}{d\rho} \approx \frac{1}{A^2(t-t_0)^2}\left(1 - 2\frac{\rho}{\rho_c}\right) \quad \text{for} \quad t \to \infty. \tag{17}$$

Already for $\rho > \rho_c/2$ the compressibility would become negative for the pure homogeneous cooling case in the asymptotic long time limit. In the standard free homogeneous cooling case (see e.g. [3]) the density dependence of the dissipation coefficient is not considered. A phenomenon reminiscent of inelastic collapse [28] is obtained, when Eq. (15) is solved at constant pressure close to $\rho = \rho_c$ and the system is allowed to contract homogeneously. In this case we obtain from (11a) $g(\rho) \approx p/(\rho_c T)$ and (15) is solved by $T = T_0(1 - A(p/\rho_c T_0)(t - t_0))^2)$, which leads to a zero granular temperature and consequently maximum packing fraction in finite time. Since the pressure stays finite in this scenario, there is no mechanism to prevent the system from going beyond the maximum packing fraction into regions with negative compressibility, which can easily be seen by setting the temperature back into the expression for the density and performing the derivative with respect to the density. The homogeneous state is never reached in simulations, since there will be spatial fluctuation of the density or the pressure.

In simulations the effect of negative compressibility appears as regions in which mass can be accumulated indefinitely. Therefore the simple kinetic model did not allow for simple filling simulations. Similar regions of negative compressibility have been found in other kinetic models of granular gases [29].

In addition to this instability, there are also indications [30], that for high densities and small granular temperatures, the viscosity should not decrease with decreasing temperature as in Eq. (11) but rather dramatically increase comparable to the behavior observed in disordered systems close to the glass transition. This discrepancy is due to neglecting collective phenomena caused by the strong repulsions of the grains.

In the following we will introduce a static pressure independent of the granular temperature and consistent modifications of the viscosity and dissipation coefficients. With these modifications the shortcomings of the purely kinetic theory will be removed and quasi static solutions will be possible.

2.4 Hybrid constitutive model

We have seen that a purely kinetic model gives rise to instabilities which we, at least in this form, do not expect to exist in reality. The problem is not so much, that there are negative compressibilities or finite times in which the maximum packing state is reached. The true problem is, that the kinetic model does not contain any mechanism to stabilize the system again. In reality, there may be transient local negative compressibilities in out of equilibrium situations, but this always leads to processes which drive the system back to thermodynamic stable states. In granular systems it is the underlying solid nature of the grains which stabilizes the contracting granular system. The zero granular temperature state at maximum packing fraction is stable due to repulsive forces between the grains and elastic forces within the grains, which limit the increase of the solid volume fraction of the granular

systems. These elastic forces are not contained in kinetic theories and at zero granular temperature the collisional pressure (11a) is zero. Consequently a resting granular system is not stable within kinetic theory, since at $T = 0$ external forces cannot not be balanced in the momentum Eq. (2).

One possibility to cure this problem is to introduce explicitely the equations for the solid granular behavior and to couple it to the hydrodynamic equations [31]. Here we will propose a simpler approach in order to limit the numerical efforts. The main reason for the observed instability was the purely collisional pressure.

In reality the pressure will have a component due to the elastically deforming grains, which is independent of the granular temperature. Instead of calculating the full strain tensor, whose trace gives rise to the elastic pressure [31], we will mimic this pressure by introducing a temperature independent but density dependent pressure p_Y which diverges at maximum packing fraction. A first attempt to create such a model was presented by Savage in [1]. We will adopt a simplified model which nevertheless captures the essential features of the more elaborate model of [1] and is able to reproduce many known experimental results of granular flow from fast to slow dense flow.

The main idea is to introduce a cross over density ρ_0, where the pressure acquires an additional contribution p_Y which is independent of the granular temperature. In the model of Savage this pressure is related to a pressure on the yield surface during quasi static deformations. Different functional dependencies on the density can be found in the literature (see [1] for a discussion of the literature). We choose for simplicity the same form as for the collisional pressure, resulting in a stronger divergence of the pressure as in [1]. Numerical tests for other dependencies did not lead to qualitatively different results. The yield pressure p_Y is given by

$$p_Y = \Theta(\rho - \rho_0) T_0 (\rho - \rho_0) g(\rho), \tag{18}$$

where Θ is the Heaviside step function. The scaled distance $\delta = (\rho - \rho_0)/\rho_0$ from the density ρ_0 may be considered as a measure for the introduced strain. The effectice elastic compressional modulus K_{eff} in this interpretation would be $K_{eff} = \rho_0 T_0 g(\rho)$. The total pressure is then written as

$$p = p_K + p_Y. \tag{19}$$

The resulting equation of state for the density as function of pressure and granular temperature is then given by

$$\rho(p, T) = \begin{cases} \rho_c \dfrac{p}{\rho_c T + p}, & p \le p_0 \\ \rho_c \dfrac{p + T_0 \rho_0}{p + \rho_c (T + T_0)}, & p > p_0 \end{cases}, \tag{20}$$

with

$$p_0 = \rho_0 T g(\rho_0). \tag{21}$$

With this choice for p_0 the density is continuous at p_0 albeit not continuously differentiable. The discontinuous compressibility does not to influence the result of our simulations qualitatively.

The transport coefficients η and λ as well as the dissipation rate ε also have to be modified to guarantee that they do not vanish with vanishing temperature. We will choose a form which makes sure that

- the viscosity is diverging with vanishing temperature, consistent with a glass transition scenario at $T = 0$ [11],
- the cross over from the kinetic to the yield regime does not modify the internal friction angle (see below in Sect. 4.1)

$$\eta := \eta_K \left(1 + \frac{p_Y}{p_K}\right) \tag{22a}$$

$$\varepsilon := \varepsilon_K \left(1 + \frac{p_Y}{p_K}\right) \tag{22b}$$

$$\lambda := \lambda_K \left(1 + \frac{p_Y}{p_K}\right). \tag{22c}$$

The mathematical form of (22) is the same as in [1]. We will show in 4.1 that it guarantees the continuity of the internal friction angle (25) at $p = p_0$.

The final equations governing the flow are given as:

$$\partial_t \rho + \operatorname{div}(\rho u) = 0 \tag{23a}$$

$$\partial_t (\rho u) + \operatorname{div}(\rho u \otimes u) - \operatorname{div}(\eta \kappa) = -\operatorname{grad}(p) + \rho \mathbf{g} \tag{23b}$$

$$\partial_t (c_p \rho T) + \operatorname{div}(u c_p \rho T) - \operatorname{div}(\lambda \operatorname{grad}(T)) = \eta \kappa : \kappa - \epsilon T. \tag{23c}$$

3 Numerical algorithm

We briefly describe the space discretization of the equations in (23) and how the resulting semi-discrete system is advanced in time. The computational domain is discretized into N finite volumes. The unknowns are located at the volume centres and each volume has $2d$ faces in the d Cartesian directions where d denotes the dimension of the space. Plainly speaking, we discretize using cell-centred bricks as volumes. The equations in (23) are first transformed to the integral form and then discretized with the help of Gauss' theorem. Convective terms are discretized using first order upwinding. Diffusive terms are then discretized as the sum of gradients over the faces multiplied by the face area where the face gradients are approximated by first order differencing using the adjacent cell center values.

3.1 Nonlinear pressure correction algorithm

After space discretization we are left with a semi-discrete system. The question arises how to numerically advance this

system in time. We argue for an implicit scheme because of the high viscosities for small temperatures and large densities. Explicit schemes would be bound to a timestep restriction of type $\tau < h^2/\eta$ where h is the scale of space discretization. For large viscosities, explicit schemes are therefore not useful.

Furthermore, we construct an algorithm around the pressure as the independent variable because pressure is allowed to vary between zero and infinity whereas the volume fraction depends on the pressure and has strict bounds between zero and random closed packing for spheres at 0.64. Numerous numerical experiments suggest that a linear pressure correction fails for our system. The highly nonlinear algebraic relations, especially in areas where the dilute and dense regimes are close introduce nonlinear terms when a pressure algorithm is derived. We decouple temperature from our system and need to fullfill (in the absence of external forces)

$$\frac{\rho(p^{n+1})u^{n+1} - \rho^n u^P}{\tau} + \operatorname{grad}\left(p^{n+1} - p^n\right) = 0$$
$$\frac{\rho(p^{n+1}) - \rho^n}{\tau} + \operatorname{div}\left(\rho(p^{n+1})u^{n+1}\right) = 0,$$

where the superscripts $n+1$ and n denote the unknown values at the current timestep and the values from the previous timestep, respectively. A velocity u^P is predicted through the linearized Navier–Stokes equation at the pressure of the previous timestep. We introduce a "nonlinear version" of the pressure operator usually applied in the linear case $\mathcal{L}(\rho^{n+1}, p^{n+1})$ and need to solve an equation of the form

$$\left[\mathcal{L} - \frac{1}{\tau^2}\right]\left(\rho(p^{n+1})\right) = \left[\mathcal{L} - \frac{1}{\tau^2}\right]\left(\rho(p^n)\right) + \frac{1}{\tau}\mathcal{D}(\rho^n u^n)$$

plus additional terms, where τ is the timestep, $\mathcal{D}$ is the discrete divergence and both $\mathcal{L}$ and ρ are nonlinear functions of the pressure. This equation is discretized in space on a cell-centred finite volume grid and solved using a Netwon-type method. Based on this new pressure, the velocity is then corrected.

Let us remark that many attempts to find a stable algorithm using a linear pressure correction type algorithm have preceded this work. We found that the nonlinearity of the equations, especially the dependence of density on pressure (20) does not allow the straightforward use of standard linear pressure correction schemes. The second problem, the need for our scheme to work in both compressible and incompressible regimes has been addressed for the linear case. We cite here exemplary [32] and [33]. However, all pressure correction methods linearise the pressure equations which in our case is not permissable. We take into account the full nonlinearity of the problem. Another type of nonlinearity in the pressure correction which is introduced through the upwind discretization of the mass flux in the compressible case is already discussed shortly in [34]. We make use of some of ideas developed there.

For a detailed mathematical description of the sketched method we refer to [13, Chap. 2].

4 Numerical experiments

In this section we will show that the presented hybrid model for granular flow can be solved with our numerical algorithm and is able to reproduce typical granular flow patterns from dilute to dense regimes. We will concentrate on the dense regime, since the model is equivalent to often tested kinetic theory in dilute and intermediately dense flow.

Let us describe the numerical setup. The space discretization, as described in Sect. 3, is a grid of finite volumes. The grid is usually refined towards the boundary, as is common practice in numerical simulations of fast flow as boundary effects are relevant there. For granular flow, boundary effects (shear bands etc.) occur also in the slow regime which is why we make use of the boundary refinement. The simulations are done using a finite volume solver framework CoRheoS developed by the authors. We solve the full nonlinear unsteady problem for each simulation. Details specific to the numerical experiment like timestep, grid resolution etc. will be given in the respective subsections following. For the constants involved in the constitutive relations we use

$$\rho_c = 0.64,\ \beta = 1.75,\ T_0 = 0.5,\ c_0 = 0.6,$$
$$\varepsilon_0 = 6754.31\frac{1}{\mathrm{s}},\ \eta_0 = 0.00023\frac{\mathrm{m}^2}{\mathrm{s}},\ \lambda_0 = 0.00034\frac{\mathrm{m}^2}{\mathrm{s}}.$$

Throughout all simulations we use no-slip boundary conditions for solid walls, i.e. we prescribe the velocity there to be zero. The effect of finite wall slip will be investigated in future publications.

4.1 Studies on the angle of repose

One of the most obvious observable properties that make granular media different from common fluids is the formation of piles. Even though the resulting angle of repose is not a material property, it is often very close to the internal friction angle which quantifies the frictional interactions of the grains.

It has been shown [11], that solid like behavior is a solution of the purely kinetic model. By solving Eq. (23) with the kinetic expression for pressure and transport coefficients (11) for a shearing experiment at constant pressure, the shear stress σ_{xy} will be proportional to the normal stress component given by the pressure p independent of the shear rate i.e

$$\sigma_{xy} = p \tan \Phi \tag{24}$$

where the tangent of the internal friction coefficient is given by

$$\tan \Phi = \sqrt{\varepsilon_0 \eta_0}. \tag{25}$$

We will now show, that we obtain the same relation with the choice of the hybrid model Eqs. (19) and (22).

For an ideal shearing experiment the coordinate system can be chosen such that the changes of the velocity are perpendicular to the direction of the velocity. If we choose the velocity $\mathbf{u} = (u(y), 0, 0)$ the only non vanishing shear stress component is $\sigma_{xy} = \eta \partial u / \partial y$. From the equation for the granular temperature neglecting gradients in the granular temperature we find from the balance of viscous heating and dissipation

$$\eta \left(\frac{\partial u}{\partial y} \right)^2 - \varepsilon T = 0. \tag{26}$$

The ratio of shear stress and pressure is given by

$$\frac{\sigma_{xy}}{p} = \frac{\eta}{p} \frac{\partial u}{\partial y}. \tag{27}$$

With Eq. (26) this can be written as

$$\frac{\sigma_{xy}}{p} = \frac{\sqrt{\eta \varepsilon T}}{p}. \tag{28}$$

Using Eqs. (18) and (22) we obtain

$$\frac{\sigma_{xy}}{p} = \frac{\sqrt{\eta_K \varepsilon_K T}}{p_K} \tag{29}$$

which gives with Eq. (11) immediately (if $\beta = 1$) expressions (24) for the purely kinetic model as well as for the hybrid model and (25) for the ratio of shear stress and normal stress. It is especially guaranteed, that the internal friction angle is continuous at $p = p_0$. The case $\beta > 1$ turns out to be numerically instable (see Sect. 4.4).

The internal friction angle may differ by a few degrees from the measured angle of repose (which varies slightly through different experiments), the formula should still suggest a range of values to match the angle of repose found in our numerical experiments.

To measure the angle of repose we simulate a Hele-Shaw-cell experiment using the hybrid model. We compute on a two-dimensional grid with 94×82 cells of cell width 1.25×10^{-2}m. The grid is uniform within the domain and is refined at the boundary to avoid that boundary effects obscure the results.

For initial conditions, we "fill" the domain with a volume fraction of sand of 1×10^{-4}. At the inflow we prescribe Dirichlet boundary conditions for the volume fraction (0.4) and the velocity in y direction (-0.5 m/s). We should mention that the whole process is simulated in one run of solving the time-dependent equations described above. This includes the free falling of grains out of the inlet as well as the formation of the pile on the bottom.

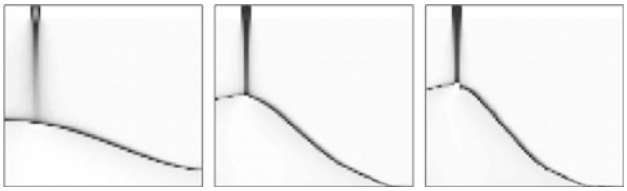

Fig. 1 Inverse colour scale visualization of the volume fraction at the final stages of filling a Hele-Shaw cell with granular media at angles, from *left* to *right*, of 23°, 40° and 48°

We run the simulation for three different internal friction angles by using three different values of $\varepsilon_0 = 6{,}750 \frac{1}{\mathrm{s}}$, $3{,}700 \frac{1}{\mathrm{s}}$ and $1{,}000 \frac{1}{\mathrm{s}}$. With Eq. (25) this results in internal friction angles Φ of 51°, 42° and 25°, respectively. The measured slopes resulting from the simulations and displayed in Fig. 1 are found to be 48°, 40° and 23°. These values are within the commonly expected proximity to the internal friction angle. The slopes are measured at medium height of the pile where the least curvature is found.

4.2 Sliding of grains on an inclined plane

Another aspect of granular flow is the transition from rest to flow depending on the magnitude of the acting force. An extensively studied experiment is the sliding of layers of granular media on an inclined plane. Depending on inclination angle, the behavior of the granular media is quite different. Below the angle of internal friction, the grains either stay at rest or only a thin surface layer begins to slide. If the inclination is increased through and above the internal friction angle, the thickness of the layer of resting material decreases. In [12], a kinetic model of granular flow is studied with regard to this aspect. A qualitative agreement to measurements is found there. Among many references, it cites [35] which gives experimental data for our comparison.

Our simulation is as follows. We study the flow in a thin cell, whose width is around 3 grain diameters of 1.75×10^{-4}m. The height of the initial resting bulk of grains is 8×10^{-3}m and rests on a 0.2 m long plane. The resolution of the grid is 2×10^{-3}m in x direction and 5×10^{-4}m in y direction. The initial conditions of resting sand are achieved by a steady state computation on the horizontal plane. Then the plane is inclined which initiates the transition from rest to flow. The thickness of the resting layer is determined by declaring all grain layers with velocity less than 1×10^{-3} m/s as not moving.

Figure 2 collects the results of our simulations as a plot of critical thickness against angle of inclination. Our simulation scenario, the tilting of static layers, corresponds to [35, Figure 1, open triangular markers]. The form of dependence

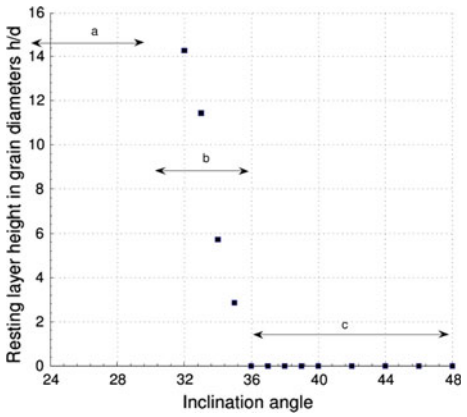

Fig. 2 Plot of the thickness of the resting layer in number of grain layers against the inclination angle in degrees. At large angles in zone (*c*) no grains stay at rest at our grain layer resolution. In zone (*b*) which is slightly above the internal friction angle of 30°, the resting layer depends strongly on the angle. At angles below, most of the grain layers rest and at significantly lower angles outside the figure extends, only a thin surface layer moves

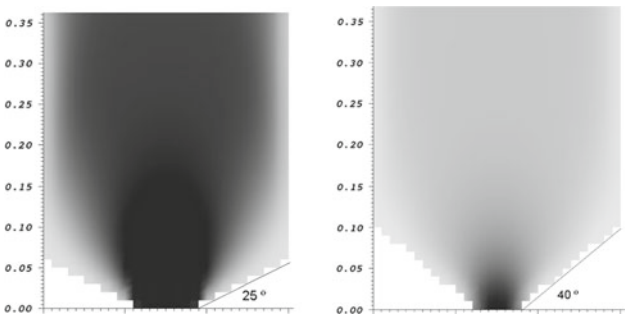

Fig. 3 Plot of an intermediate stage in the process of emptying a silo. We plot the magnitude of the mass flux where dark areas mean a large mass flux. In the *left* silo (25°) we observe a large difference in mass flux between the center and the side zones above the end of the hopper. In the *right* silo we observe homogeneous flow throughout most of the silo. The *y*-axis shows the height in m

of resting layer thickness on the inclination angle from our simulation is in very good agreement with the experimental findings therein. At angles above 36°, the authors of [35] find a resting layer of 2 grain diameters thickness which is below our resolution. Hence in our simulations we obtain no resting layer at all for these angles.

We want to point out that in further agreement with experiments the thickness of the resting layer approaches zero for angles significantly above the internal friction angle, where in [12] the thickness seems to become small but finite (see [12, Fig. 1]).

It is reported that there is a difference between the critical heights for the transition from resting to flowing on one side and from flowing to resting on the other side (see experiments cited in [36]). This difference is similar to the difference between static and sliding friction. Since static Coulomb friction is not yet included in the model, we assume that it is currently not possible to obtain this difference in our simulations.

4.3 Core- and massflow during emptying of silos

Simulation of granular media finds a wide range of applications in the field of handling of bulk goods. The vast majority of simulations in this area is carried out using DEM methods, treating each grain as a separate particle. The drawback of this method is the amount of grains that would need to be simulated for a full hopper. For a hopper of industrial size, a realistic estimate is 1×10^9 to 1×10^{12} particles which is out of the reach of current computation equipment by many orders of magnitude. Certainly there may be effects that can only be simulated by accounting for single particle interactions, but those have to be restrained to much smaller scales. With our method, we can simulate the complete process of emptying an industry-sized hopper in days on standard non-parallel workstation hardware.

A basic effect of silo flow is the distinction of core and mass flow depending on the steepness of the silo cone. For flat silos, so called core flow occurs where stagnation zones occur close to the bottom of the silo and the mass flux is concentrated more towards the center of the silo. For steep silos, the grains at every point in the silo flow downwards, no inverse cone in the center is observable and mass flow occurs.

We simulate the emptying of two silos with different inclination angles of the cone. The internal friction angle of the granular material is around 30°. The simulations are carried out for inclination angles of 25° and 40°. Experiments suggest that we can expect to observe coreflow (i.e. stagnation zones) for the flat angle and mass flow for the larger angle. Our results show exactly this behavior in Fig. 3. The difference between mass flow and core flow can clearly be seen. In addition we observe in the simulation that in the case of mass flow, the flux vectors are directed parallel to the direction of gravity at every point in the silo where in the case of core flow the grains on the top slide into the middle of the silo and mostly from there slide downward.

For a more detailed investigation of the stagnation zones found in the left silo of Fig. 3 we provide flux profiles at different heights of the silo. This shows that from the simulations a distinct structure of the stagnation zones can be extracted (Fig. 4).

4.4 Instabilities in the model transition for values of $\beta > 1$ and the issue of shear bands

Bocquet et. al. show in [11] that values of β larger than 1 allow to distinguish asymptotically between a wall dominated regime and a bulk regime. As a consequence the

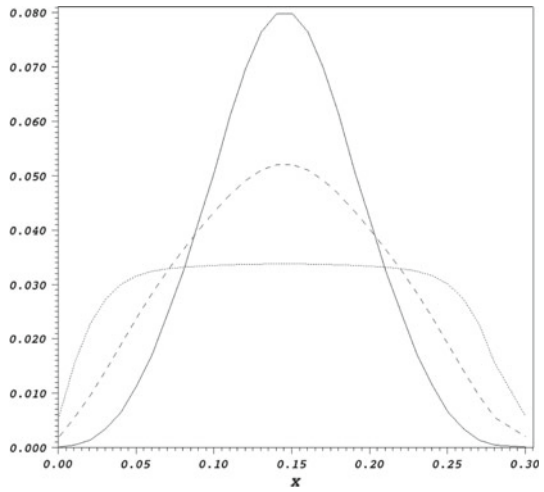

Fig. 4 Profiles of mass flux along the x-axis of the 25° silo from Fig. 3 at heights 0.07 m (*solid line*), 0.11 m (*dashed line*) and 0.3 m (*dotted line*) above the hopper bottom opening. The unit of the mass flux is $\frac{\mathrm{m}}{\mathrm{s}}$ because the density is normalized to the specific density $\hat{\rho}_s$ of the grains

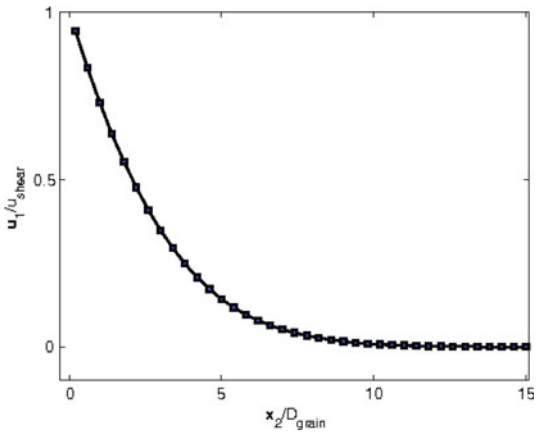

Fig. 5 Granular velocity plotted against the distance from the wall in grain layers. The shear band can clearly be seen

occurrence of shear bands is relatively easy explained for $\beta > 1$. In agreement with these arguments also our simulation reproduce shear bands for $\beta > 1$. But as Fig. 5 shows, shear bands are within the hybrid model also recovered for $\beta = 1$. The width of the band is in quantitative agreement with the experimental results of [11, Fig. 2].

In the simulation of heap formation the choice $\beta > 1$ is causing strong deviations between angle of repose and internal friction angle. In Fig. 6 it is seen that for the suggested value of $\beta = 1.75$, the angle of repose in the formed pile is much steeper than the internal friction angle, which is chosen to be around 40°. This mismatch of the dynamic angles of repose in the different regimes of the hybrid constitutive model (Sect. 2.4) is a feature we observed in all simulations with $\beta > 1$. Only for $\beta = 1$, a consistent internal friction

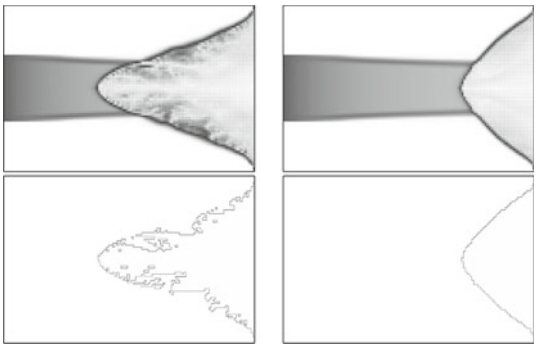

Fig. 6 Experiment showing the difference in pile formation between $\beta = 1$ (*right*) and $\beta = 1.75$ (*left*). In the plots on the *top*, the volume fraction is displayed from light (low volume fraction) to dark (high volume fraction). On the *bottom*, we display the boundary between the cells in which the constitutive relations (22) (dense regime) are active and those in which the constitutive relations derived from kinetic theory (Sect. 2.2) are active

angle is found throughout the whole range of volume fractions.

Even more serious is the occurrence of an instability if $\beta > 1$ is used within the hybrid model. The instability shows up in a fractal like density variation close to the surface of the heap. The fractal is seen even more clearly when plotting the boundary between the constitutive relations of the dense regime and the kinetic regime (see Fig. (6)). During the simulation fluid like regions appear at the surface of the heap and propagate from the surface into the heap until dying out again due to the energy dissipation. As a consequence strongly fluctuating surfaces are observed during the heap formation. We believe that the effect is caused by the velocity weakening regime which exists for very large density if β is larger than 1 [12]. We want to point out, that a constant angle of repose should be obtained, if the density divergence in the dissipation ε is modified to $\varepsilon \propto g(\rho)^{2-\beta}$. This is not excluded by glass transition theory cited in [11]. Only the pressure should not show any anomalous divergence. Further investigations of the observed instability are planned for future publications.

5 Conclusion

We have studied in this work a model for granular flow in all regimes (dilute to dense) and presented a stable discretization and solution algorithm for this model. The model together with the algorithm was challenged against a selection of test problems and succeeded to qualitatively reproduce phenomena like shear bands, angles of repose, stagnation points in hopper flow to name a few. Thus we showed that the model is capable to recover essential phenomena observed in granular flow from dilute to dense regimes. Our model is certainly not

unique. Many similar models are conceivable with different forms of the yield pressure and the transport coefficients. In this respect, one important result of our research is the numerical method which allows to investigate these variations in the future. It remains to be studied to which extent anisotropic distributions of static stresses are already covered by this class of models. The addition of a static pressure with consistent modifications of the viscosity and the dissipation coefficients will certainly not be enough to fully capture the complex behavior of solid like granular matter. Besides a more quantitative validation of the used model, the constitutive relations and their analytical form, also the instability discussed in Sect. 4.4 will be investigated in more details in the future.

Acknowledgments The research was sponsored in part by the German Federal Ministry of Education under Grant number 01 RI 05008, supervised by the Project Management Agency at the DLR Bonn. We are grateful to D. Niedziela for communicating to us the results on the effect of the bulk viscosity on the simulations and the simulation of the shear flow experiments which require special care in numerical implementation.

A Variation of the temperature at constant pressure

The equation for the granular temperature within kinetic theory is derived using the Boltzmann equation for inelastically colliding particles. The energy of the particles is just the kinetic energy. The resulting equation for the fluctuation of the kinetic energy density $U = c_v \rho T$, which is identical to the internal energy density of the colliding gas gives in Lagrangian notation [3]

$$c_v \rho \left(\frac{dT}{dt}\right) = -\hat{\rho}_s \nabla \mathbf{q} - p_s \nabla \mathbf{u} + \underline{\underline{\sigma}}^D : \underline{\underline{\kappa}} - \frac{3}{2}\rho\varepsilon T, \qquad (30)$$

where $c_v = 3/2$ is the specific heat at constant volume. c_v is unitless since due to the lack of a granular Boltzmann constant the granular temperature is defined as $T = \langle(\delta v)^2\rangle$, where the brackets indicate average over the Boltzmann distribution. We note that the equation does not coincide with the usual form obtained from macroscopic hydrodynamic considerations [14] due to the appearance of $p_s \nabla \mathbf{u}$. The origin for the discrepancy is the fact, that the Boltzmann equation is solved in zeroth order by the canonical distribution function f_{eq}

$$f_{eq} = f_0 \exp\left(-\frac{m(\mathbf{u} - \langle \mathbf{u}\rangle)^2}{2k_B T}\right) \qquad (31)$$

i.e. Eq. (30) is valid for processes at constant volume, instead of constant pressure. Note, that the term $\nabla \mathbf{u}$ is proportional to a change in the volume

$$\nabla \mathbf{u} = \frac{1}{V}\frac{dV}{dt} = -\frac{1}{\rho}\frac{d\rho}{dt}. \qquad (32)$$

Consequently the term in (30) proportional to the pressure p_s should not contribute to the change of the granular temperature. To obtain the equation for temperature changes at constant pressure within Boltzmann theory it would be necessary to derive the equation for the enthalpy $H = U + p_s V$. Here we motivate Eq. (4), assuming (30) to be valid also for constant pressure and constraining it to changes at constant pressure.

The time change of the enthalpy at constant pressure per unit volume is given by

$$c_p \rho \frac{dT}{dt} = \frac{1}{V}\frac{dH}{dt} = \frac{1}{V}\frac{dU}{dt} - \frac{p_s}{\rho}\frac{d\rho}{dt} = \frac{3}{2}\rho\frac{dT}{dt} - \frac{p_s}{\rho}\frac{d\rho}{dt} \qquad (33)$$

where c_p is the specific heat at constant pressure per unit mass. Considering the pressure as a function of temperature and density $p_s = p_s(\rho, T)$, the change dp_s in the pressure can be written

$$dp_s = \frac{\partial p_s}{\partial \rho}|_T \, d\rho + \frac{\partial p_s}{\partial T}|_\rho \, dT. \qquad (34)$$

In a Lagrangian formulation we obtain with (32) and (34) at constant pressure (i.e. $dp_s = 0$)

$$-p_s \nabla \mathbf{u} = \frac{p_s}{\rho}\frac{d\rho}{dt} = -\frac{p_s}{\rho}\left(\frac{\frac{\partial p_s}{\partial T}|_\rho}{\frac{\partial p_s}{\partial \rho}|_T}\right)\frac{dT}{dt}. \qquad (35)$$

Replacing $\nabla \mathbf{u}$ in (30) by (35) and using (33), Eq. (30) is at constant pressure transformed into (4).

References

1. Savage, S.B.: Analysis of slow high-concentration flows of granular materials. J. Fluid Mech. **377**, 1–26 (1998)
2. Kadanoff, L.P.: Built upon sand: theoretical ideas inspired by granular flows. Rev. Mod. Phys. **71**(1) (1999)
3. Brilliantov, N.V., Pöschel, T.: Kinetic Theory of Granular Gases. Oxford Graduate Texts. Oxford University Press, Berlin (2003)
4. Luding, S., McNamara, S.: How to handle the inelastic collapse of a dissipative hard-sphere gas with the tc model. Granul. Matter **1**(3), 113–128 (1998)
5. Luding, S.: On the relevance of molecular chaos for granular flows. ZAMM **80**, 9–12 (2000)
6. Gidaspow, D.: Multiphase Flow and Fluidization. Academic Press, New York (1994)
7. Khain, E., Meerson, B.: Onset of thermal convection in a horizontal layer of granular gas. Phys. Rev. E **67**(2), 021,306 (2003)
8. Carrillo, J.A., Pöschel, T., Saluena, C.: Granular hydrodynamics and pattern formation in vertically oscillated granular disk layers. J. Fluid Mech. **597**(1), 119–144 (2008)
9. Meerson, B., Pöschel, T., Bromberg, Y.: Close-packed floating clusters: granular hydrodynamics beyond the freezing point? Phys. Rev. Lett. **91**(2), 024301 (2003)
10. Meerson, B., Díez-Minguito, M., Schwager, T., Pöschel, T.: Close-packed granular clusters: hydrostatics and persistent gaussian fluctuations. Granul. Matter (10), 21–27 (2007)

11. Bocquet, L., Losert, W., Schalk, D., Lubensky, T.C., Gollub, J.P.: Granular shear flow dynamics and forces: experiment and continuum theory. Phys. Rev. E **65**(1), 011307 (2001)
12. Bocquet, L., Errami, J., Lubensky, T.: Hydrodynamic model for a dynamical jammed-toflowing transition in gravity driven granular media. Phys. Rev. Lett. **89**, 184301 (2002)
13. Schmidt, S.: On numerical simulation of granular flow. Ph.D. thesis, Technische Universität Kaiserslautern http://kluedo.ub.uni-kl.de/volltexte/2009/2364/ (2009)
14. Landau, L., Lifshitz, E.M.: Fluid Mechanics, Course of Theoretical Physics, vol. 6. Pergamon Press, Oxford (1987)
15. Garzo, V., Dufty, J.W.: Dense fluid transport for inelastic hard spheres. Phys. Rev. E **59**, 5895–5911 (1999)
16. Luding, S.: Global equation of state of two-dimensional hard sphere systems. Phys. Rev. E **63**(4), 042201 (2001)
17. Garcia-Rojo, R., Luding, S., Brey, J.J.: Transport coefficients for dense hard-disk systems. Phys. Rev. E Stat. Nonlinear Soft Matter Phys. **74**(6), 061305 (2006)
18. Khain, E.: Hydrodynamics of fluid-solid coexistence in dense shear granular flow. Phys. Rev. E Stat. Nonlinear Soft Matter Phys. **75**(5), 051310 (2007)
19. Luding, S.: Towards dense, realistic granular media in 2d. Nonlinearity **22**(12), R101–R146 (2009)
20. Fingerle, A., Herminghaus, S.: Equation of state of wet granular matter. Phys. Rev. E Stat. Nonlinear Soft Matter Phys. **77**(1), 011306 (2008)
21. Dahler, J.S.: Transport phenomena in a fluid composed of diatomic molecules. J. Chem. Phys. **30**, 1447–1475 (1959)
22. Campbell, C.S.: Boundary interaction for two dimensional granular flows. part1. flat boundaries, asymmetric stresses and couple stress. J. Fluid Mech. **247**, 111–136 (1993)
23. Mitarai, N., Hayakawa, H., Nakanishi, H.: Collisional granular flow as a micropolar fluid. Phys. Rev. Lett. **88**(17), 174301 (2002)
24. Landau, L., Lifshitz, E.M.: Fluid Mechanics, Course of Theoretical Physics, vol. 7. Pergamon Press, Oxford (1986)
25. Hansen, J.P., McDonald, I.R.: Theory of Simple Liquids. Academic Press, New York (1986)
26. Khain, E., Meerson, B.: Shear-induced crystallization of a dense rapid granular flow: hydrodynamics beyond the melting point. Phys. Rev. E Stat. Nonlinear Soft Matter Phys. **73**(6), 061301 (2006)
27. To be more precise for constant volume the specific heat should be replaced by the specific heat at constant volume
28. McNamara, S., Young, W.R.: Inelastic collapse in two dimensions. Phys. Rev. E **50**(1), R28–R31 (1994)
29. Khain, E., Meerson, B.: Symmetry-breaking instability in a prototypical driven granular gas. Phys. Rev. E **66**(2), 021306 (2002)
30. D'Anna, G., Mayor, P., Barrat, A., Loretto, V., Nori, F.: Observing brownian motion in vibration-fluidized granular matter. Nature **424**, 909–912 (2003)
31. Jiang, Y., Liu, M.: Granular solid hydrodynamics. Granul. Matter **11**(3), 139–156 (2009)
32. Churbanov, A.: A Unified Algorithm to Predict Compressible and Incompressible Flows and Incompressible Flows. Lecture Notes in Computer Science, vol. 2542/2003. pp. 412–419. Springer, Berlin (2003)
33. van der Heul, D., Vuik, C., Wesseling, P.: A conservative pressure-correction method for flow at all speeds. Comput. Fluids **32**(8), 1113–1132 (2003)
34. Gastaldo, L., Babik, F., Herbin, R., Latche, J.C.: An unconditionally stable pressure correction scheme for barotropic compressible navier-stokes equations. In: ECCOMAS CFD (2006)
35. Daerr, A., Douady, S.: Two types of avalanche behaviour in granular media. Nature **399**, 241–243 (1999)
36. GDR-MiDi: On dense granular flow. Eur. Phys. J. E **14**, 341–365 (2004)